



HAL
open science

Charge ordering in two-dimensional ionic liquids

Aurélien Perera, Tomaz Urbic

► **To cite this version:**

Aurélien Perera, Tomaz Urbic. Charge ordering in two-dimensional ionic liquids. *Physica A: Statistical Mechanics and its Applications*, 2018, 495, pp.393 - 404. 10.1016/j.physa.2017.12.076 . hal-01688438

HAL Id: hal-01688438

<https://hal.sorbonne-universite.fr/hal-01688438>

Submitted on 19 Jan 2018

HAL is a multi-disciplinary open access archive for the deposit and dissemination of scientific research documents, whether they are published or not. The documents may come from teaching and research institutions in France or abroad, or from public or private research centers.

L'archive ouverte pluridisciplinaire **HAL**, est destinée au dépôt et à la diffusion de documents scientifiques de niveau recherche, publiés ou non, émanant des établissements d'enseignement et de recherche français ou étrangers, des laboratoires publics ou privés.

Charge ordering in two-dimensional ionic liquids

Aurélien Perera¹ and Tomaz Urbic²

¹Laboratoire de Physique Théorique de la Matière Condensée (UMR CNRS 7600), Université Pierre et Marie Curie, 4 Place Jussieu, F75252, Paris cedex 05, France.

²Faculty of Chemistry and Chemical Technology, University of Ljubljana, Vecna pot 113, 1000 Ljubljana, Slovenia.

Abstract

The structural properties of model two-dimensional (2D) ionic liquids are examined, with a particular focus on the charge ordering process, with the use of computer simulation and integral equation theories. The influence of the logarithmic form of the Coulomb interaction, versus that of a 3D screened interaction form, is analysed. Charge order is found to hold and to be analogous for both interaction models, despite their very different form. The influence of charge ordering in the low density regime is discussed in relation to well known properties of 2D Coulomb fluids, such as the Kosterlitz-Thouless transition and criticality. The present study suggests the existence of a stable thermodynamic labile cluster phase, implying the existence of a liquid-liquid “[transition](#)” above the liquid-gas binodal. The liquid-gas and Kosterlitz-Thouless transitions would then take place inside the predicted cluster phase.

1 Introduction

Two-dimensional fluids, although being of academic interest, provide an interesting system to study the influence of fluctuations on the stability of different phases[1], and in particular through the structural properties. Indeed, dimensionality plays a crucial role in the existence and nature of phase transitions[2]. Similarly, dimensionality conditions the form of the Coulomb interaction, through the

solution of the Poisson equation[3]. In two-dimensions, this solution imposes that the Coulomb interaction is logarithmic[3, 4]. This is particularly serious at large separations since the interaction is diverging. [In particular, it leads to the well known Kosterlitz-Thouless \(KT\) topological transition\[6\] at low density, when all charges are found to bind below the transition temperature. This is not the case in 3 dimension.](#) However, in a dense liquid state, the short range effects, both in the interactions and the correlations are equally important, and one interesting question is what is the relative importance of long range versus short range in the specific properties of a fluid. This question becomes particularly interesting in two-dimensions than in three-dimensions, because of the particular form of the Coulomb interaction and the greater importance of fluctuations because of the reduced dimensionality.

Charge order in liquids is the result of the Coulomb interaction and is particularly observed through pair correlation functions. It has been discussed in early studies of charged liquids[5], but lost relevance in later papers. In recent studies[7, 8], we have shown the importance of Coulomb interaction induced charge ordering in three-dimensional liquids. In particular, we have shown how the perturbation of charge order by inert chemical atomic methyl groups could affect the physico-chemical properties. The most apparent such property is the fact that pure charges are crystalline at room temperature, while charges chemically complexified with neutral groups, the so-called room temperature ionic liquids[9], are liquid at room temperature. In the same study, we have shown that approximate integral equation theories could be very accurate in predicting structural properties. The question naturally arise as to whether these theories would remain accurate when lowering the dimensionality. Indeed, lowering the dimensionality increases the importance of fluctuations, the latter which play an important role in the stability of the system. Interestingly, as far as simple liquids are concerned, such as those made of hard particles and attractive particles, approximate theories such as integral equations, namely the hypernetted chain (HNC), or the Percus-Yevick theory, have about the same level of accuracy in three and two dimensions[10, 11]. In the case of core softened interactions, the HNC theory proved even very accurate[12]. The diagrammatically lower level Percus-Yevick approximation becomes exact for hard discs in one-dimension[13]. These issue indicates that the statistical description of the short range structure and that of fluctuations are distinct, despite being related through the link between stability and corresponding integral of the correlation functions, which is the essence of the fluctuation dissipation theory. We consider this issue to be crucial to understand the appearance of complexity in liquids, such as clustering and micro-heterogeneity. In the present work we set up to explore some aspects of this problem through the analysis of a two dimensional ionic liquid in its simplest form, namely a binary mixture of charged soft discs. We focus here on the short

range order, namely the charge order, and the ability of theory to describe the structure accurately. A closely related system, the charged hard disc binary mixture, so called two-dimensional restricted primitive model (2D-RPM), has been abundantly studied in the past[14, 15, 18, 19, 20, 21, 22, 23, 24], namely in the low density low temperature region of the phase diagram, where the Kosterlitz-Thouless transition takes place[25], as well as the liquid-gas transition[26]. These transitions have been originally studied from very different view points. The KT transition[6] is originally a model for how topological defects (or dislocations) in the two-dimensional XY model appear and merge into associated pairs, separating the conducting phase from the dielectric phase[27, 28]. One peculiarity of this transition is that it is of infinite order, and it appears in a large variety of physical systems[27]. The liquid-vapour coexistence was initially a problem of accurate determination through computer simulations[26]. Both these transitions seem to have over shadowed the special form of ordering, namely charge order, which occurs on the dense liquid part of the phase diagram. In the present paper, we explore also the link between charge order and these two phase transitions. In particular, we explore the role of the short versus long range parts of the Coulomb interaction in all these phenomena.

2 Models, theoretical and computational details

The two-dimensional Coulomb interaction has a logarithmic singularity at large separations. In the dense fluid regime, the pair interaction is always screened at large separations. At small densities however, this is no more the case, and the logarithmic form leads to irreversible attraction of opposite charges at low temperatures, leading to the existence of a dielectric phase. These two distinct behaviour pose the problem of charge order differences at short and long ranges, particularly when the density is varied. We examine here what can be said about these issues from theoretical point of view.

2.1 Interactions and Models

The Coulomb interaction in two-dimension is obtained from the a -dimensional Poisson equation, which imposes the logarithmic form[3]. Here, we consider a fluid made of soft discs of diameter σ , and the total interaction between two discs i and j with respective valences Z_i and Z_j is set to be:

$$v_{ij}(r) = -Z_i Z_j q^2 \ln\left(\frac{r}{a}\right) + 4\epsilon \left(\frac{\sigma}{r}\right)^{12} \quad (1)$$

where a is a scaling distance, which contributes to an arbitrary gauge of the energy. We discuss below in Section 2.2 how we choose this parameter. q is an elementary two-dimensional “charge” and ε is the energy parameter of the soft interaction. Clearly, q^2 must have the dimension of an energy. To set its value, we compare with the three-dimensional case

$$v_{ij}^{(3D)}(r) = Z_i Z_j \frac{e^2}{4\pi\varepsilon_0\sigma} \left(\frac{\sigma}{r}\right) + 4\varepsilon \left(\frac{\sigma}{r}\right)^{12} \quad (2)$$

The comparison between the two equations suggests $\Gamma = q^2 = e^2/(4\pi\varepsilon_0\sigma)$. If we choose $\sigma = 3\text{\AA}$, which corresponds roughly to the diameter of the water molecule in several models, then one can show that [7] $\Gamma/k_B = T_C$, with $T_C \approx 55740\text{K}$, where k_B is the Boltzmann constant, suggesting that $\Gamma = q^2$ has indeed the dimension of an energy. We introduce the two interaction models we will be using here, written in a non-dimensional form by scaling the energies by ε , that is setting $\Gamma = \Gamma/\varepsilon$ and $\varepsilon = 1$. If we choose $\varepsilon/k_B = 100\text{K}$ (which is relatively close to the value used in many water models), this choice sets the value of the Γ parameter we will use in this work, namely $\Gamma = \Gamma_1 = 557$. With this choice, the interactions in reduced units of the two models are:

$$\beta v_{ij}(r) = -Z_i Z_j \frac{\Gamma_1}{\tau} \ln\left(\frac{r}{a}\right) + \frac{4}{\tau} \left(\frac{\sigma}{r}\right)^{12} \quad \text{Model 1} \quad (3)$$

and

$$\beta v_{ij}(r) = Z_i Z_j \frac{\Gamma_2}{\tau} \frac{\exp(-r/\lambda)}{r/\sigma} + \frac{4}{\tau} \left(\frac{\sigma}{r}\right)^{12} \quad \text{Model 2} \quad (4)$$

where $\tau = T/(\varepsilon/k_B)$ is the standard Lennard-Jones reduced temperature. We introduce reduced temperatures adapted to our models as $\Theta_1 = \tau/\Gamma_1$ and $\Theta_2 = \tau/\Gamma_2$, which fixes the leading coefficient in front of the charge term, with $\Gamma_2 = \sigma\Gamma_1$. Model 2 represents a screened version of the 3D-Coulomb interaction, it decays rapidly instead of the logarithmic divergence of Model 1. We choose here $\lambda = 2\text{\AA}$.

Both models have in common that, at short range, the Coulomb interaction dominates the soft interaction by the factor $\Gamma_1 = 557$. The models differ at long range through the presence or absence of the screening. One purpose of this work is to examine the relative weight of these two contributions. In particular, does the short range Coulomb influences the low-density low-temperature behaviour in similar manner, particularly in what concerns the Kosterlitz-Thouless transition.

2.2 Liquid state Integral Equation theory

In this work we use the hypernetted chain (HNC) approximation in order to obtain the pair correlation functions

$$g_{ij}(r) = \exp[-\beta v_{ij}(r) + h_{ij}(r) - c_{ij}(r)] \quad (5)$$

The large distance logarithmic singularity of $v_{ij}(r)$ for Model 1 is handled through the exact relation for the direct correlation functions

$$\lim_{r \rightarrow \infty} c_{ij}(r) = -\beta v_{ij}(r) \quad (6)$$

Using this relation, we write the direct correlation function of Model 1 in separating out the well behaved short range part $c_{SR;ij}(r)$ from the large distance ill-behaved part

$$c_{ij}(r) = c_{SR;ij}(r) + c_{LR;ij}(r) \quad (7)$$

with[19]

$$c_{LR;ij}(r) = Z_i Z_j \frac{\Gamma}{T} \left[\ln\left(\frac{r}{a}\right) + K_0\left(\frac{r}{a}\right) \right] \quad (8)$$

where $K_0(x)$ is the modified Bessel function of integer order. This function decays exponentially at large x , and for small x it behaves as $K_0(x \rightarrow 0) = \ln(2) - \gamma - \ln(x)$, where $\gamma \approx 0.5722$ is the Euler constant. Hence, the logarithmic singularity at $r = 0$ of the log term is canceled. The crucial parameter a is determined from the constraint that $g_{ij}(r) = 0$ for $0 < r < a$, which correspond to distance within the hard core part of the discs. We choose a from the criteria $\exp[-\beta v_{+-}(a)] = 10^{-5}$.

It is important to note that, because of the term $-\beta v_{ij}(r) + c_{ij}(r)$ in the HNC closure Eq.(5), and the choice of $c_{LR;ij}(r)$ in Eq.(8), the exponential does not have any singularities, neither at $r \rightarrow \infty$, nor at $r \rightarrow 0$. The latter singularity is in fact handled through the exact relation

$$g_{ij}(r) = 0 \quad r < a \quad (9)$$

Therefore, any Coulomb contribution can only come from the non-singular short range part, and not from the long range part. This is the principal reason why one can try other forms of the charge interactions, such as in Model 2 Eq.(4), which do not necessarily obey the Poisson equation. Moreover, the absence of the Coulomb singularities in $g_{ij}(r)$ leads one to ask how typical two-dimensional phenomena such as the KT transition can manifest through the correlation functions.

The HNC equation must be solved for the functions $h_{ij}(r)$ and $c_{ij}(r)$ in conjunction with the Ornstein-Zernike equation, which is written in the Fourier space under the following matrix form

$$\mathbf{SM} = \mathbf{I} \quad (10)$$

where \mathbf{S} is the matrix of the structure factors

$$S_{ij}(k) = \delta_{ij} + \sqrt{\rho_i \rho_j} \tilde{h}_{ij}(k) \quad (11)$$

and \mathbf{M} is related to the direct correlation function through

$$M_{ij}(k) = \delta_{ij} - \sqrt{\rho_i \rho_j} \tilde{c}_{ij}(k) \quad (12)$$

\mathbf{I} is the unity matrix, and the tilde designate the Fourier transform in two-dimensions, defined as

$$\tilde{f}(k) = 2\pi \int_0^\infty r dr f(r) J_0(kr) \quad (13)$$

where $J_0(x)$ is the Bessel function of integer order. In the case of Model 1 we note that the Fourier transform of $c_{LR;ij}(r)$ is well defined :

$$\tilde{c}_{LR;ij}(k) = -Z_i Z_j \kappa_0^{-2} \frac{2k^2 + a^{-2}}{k^2(k^2 + a^{-2})} \quad (14)$$

where $\kappa_0 = \sqrt{k_B T / (2\pi\Gamma)}$ is the Debye length in 2 dimensions. Clearly, $\tilde{c}_{LR;ij}(r)$ has the $1/k^2$ singularity at $k=0$. This singularity enforces the following Stillinger-Lovett (SL) sum rules[32] for the $\tilde{h}_{ij}(k)$, which is the way the Coulomb singularity enters the correlation functions.

$$\sum_j Z_j \rho_j \tilde{h}_{ij}^{(0)} = -Z_i \quad (15)$$

$$\sum_{ij} Z_i Z_j \rho_i \rho_j \tilde{h}_{ij}^{(2)} = \kappa_0^{-2} \quad (16)$$

where $\tilde{h}_{ij}^{(2n)} = (-1)^n \frac{1}{4^n [n!]^2} \int d\vec{r} h_{ij}(r) r^{2n}$ are the $2n$ -order moments of $\tilde{h}_{ij}(k)$ in the small- k Taylor expansion. These relations are not obeyed in the case of Model 2 since there is no Coulomb interaction in this case. Hence; we can appreciate how charge order is obeyed in both models while SL relations are violated in the second one.

The integral equation is solved using standard techniques developed for the 2D case[10]. The correlation functions are sampled on a logarithmic grid of 1024 points, and the Fourier transforms are handled through the Talman technique[29, 30].

2.3 The Kosterlitz-Thouless transition and the small density limit

The OZ equation, which is an exact equation[31], and the HNC equation, which becomes exact at low densities, show that, when $\rho = 0$, the obvious solution for all temperatures is

$$h_{ij}(r) = c_{ij}(r) = f_{ij}(r) = \exp(-\beta v_{ij}(r)) - 1 \quad (17)$$

where $f_{ij}(r)$ is the Mayer function. However, for Coulomb interactions, one sees from Eq.(1) that the cross Mayer function $f_{+-}(r)$ is asymptotically ill-defined because it diverges as $r^{\Gamma/k_B T}$ for large distances. However, the correlation functions $h_{ij}(r)$ and $c_{ij}(r)$ are always well behaved asymptotically as $\rho \rightarrow 0$. One way to conciliate these two contradictory results is that the system of free charges undergoes a phase transition to a dielectric phase in the low density region. This is the principal reason why the solution at $\rho = 0$ *must* be singular at low temperatures. In other words, for purely mathematical reasons, we expect a physical singularity to arise in the regime $\rho = 0$ and $T = 0$. The KT transition is precisely such a transition, and it arises at an universal small temperature $k_B T / \Gamma = 1/4$ [6]. It should be noted that this universality is entirely related to the 2D Coulomb form of the interaction[6, 27, 28].

This problem is obviously avoided with Model 2, since the interaction is well behaved asymptotically. The absence of long range Coulomb interaction lead to the existence of free charges at all temperatures, even in the very low density region. However, what happens to charge ordering in the low density low temperature region? Surely, due to the strong short range attraction in Model 2 we expect the existence of clusters below some temperature. The calculations conducted in the present work seem to suggest that the integral equations fail at some low temperature both for Model 1 and Model 2, and in very similar manner. **This could be related to the fact that, through Eq.(6), the long range features of Model 1 and Model 2 are cancelled in Eq.(5) in a similar fashion.** The failure of the integral equation theory is usually associated to the proximity of a phase transition, more precisely the existence of a spinodal line signaling the instability of the current phase. From this fact, one is led to speculate that the low temperature failure for both the Coulomb interaction of Model 1 and that of Model 2, could have the same origin, namely the clustering of charges, with the difference that these clusters would reduce strictly to dipolar pairs at low density in the case of Model 1. Screening the Coulomb interaction would then lead a larger clustering form -more polydisperse than dipoles, precursor of the liquid-gas phase separation predicted from computer simulations. This is the hypothesis that our results below seem to suggest. **It should be noted, however, that the cluster region may not be a true phase in the thermodynamic sense. Such non-thermodynamic “cluster phases” are**

found, for example, in many real real systems as well in models with short range attraction and long range repulsion.

2.4 Monte Carlo simulations

We perform Monte Carlo (MC) simulations in the canonical (NVT) ensemble [34] of the model where particles interact by a screened version of the 3D-Coulomb interaction. The periodic boundary conditions and the minimum image convention were used to mimic an infinite size of the system of particles. Starting configurations were selected randomly. At each step, we tried to translate a randomly chosen particle, each with the same probability. A MC cycle which corresponds to N moves of particles. Average quantities are computed from 10^7 MC cycles that are performed after an equilibration period of 10^6 cycles. Thermodynamic quantities such as energy were calculated as statistical averages over the course of the simulations [34]. Cut off of the potential was half-length of the simulation box. All simulations were performed with $N = 100$ or $N = 200$ molecules. To fix the ideas, 100 molecules is equivalent to about 1000 particles in 3D. Increasing the number of particles had no significant effect on the calculated quantities. The Monte Carlo moves in the cluster region have been performed with the same particle move algorithm. The problems posed by the hard core part of discs is avoided here since the interaction is continuous. Moreover, in this work we did not explore by simulation the very low density region, where cluster moves rather than particle moves have been suggested[35].

3 Results

Fig.1 illustrates the various components of the interactions used in this work. The blue curve represents the $1/r^{12}$ repulsive term. The magenta curve represents the 2D Coulomb interaction between opposite charge. The two green curves represent the Yukawa repulsive term for $\lambda = 1$ (dark green) and $\lambda = 2$ used in this work. It is seen that the true and effective charge interactions have seemingly very different forms, and yet they produce very similar correlations, which means very similar particle distributions in the configurational space.

3.1 Phase diagram

Fig.2 shows the (ρ, Θ) phase diagram, or rather the no-solution diagram in what concerns the HNC theory. Data from previous reports for the 2D-RPM model are shown[21, 26], namely the liquid-gas coexistence curve[26] (black), the conductor-dielectric separator (red curve) and the HNC results (blue curve). The green curve

represents the present results for Model 1 and the yellow curve for Model 2. The inset shows a zoom of the very small density region in logarithmic scale for the density, which enhances the shape similarities of the 3 no-solution curves of HNC. It is seen that the HNC no-solution curve of model 1 is quite close that of the 2D-RPM. This is expected since both repulsive interactions produce very similar structure factors in the 3D case, and it is mostly a packing effect. Indeed, since soft discs can interpenetrate, they would experience the Coulomb association at higher temperatures than the hard disc fluid. Hence, at fixed density, one expects that the no-solution would occur at a somewhat higher temperature than the equivalent hard disc system. This is what we observe here, at least in the high density region. At lower density, the turnover peak is higher and at a lower density, but both curves seem to converge towards the same limit for $\rho = 0$. This is the KT limit, at $\Theta = 0.25$ [6] We observe that Model 1 tends to this limit from above the RPM results.

Model 2 has a no-solution line (shown in yellow) well below the true Coulomb one, but above the 2D-RPM liquid-gas coexistence predicted from simulations (black curve). This is consistent with screened Coulomb liquid-gas coexistence being above that of pure Coulomb in 3D binary Yukawa mixtures[16, 17]. For this model, we do not expect a KT behaviour at low densities, but an ordinary liquid-gas transition at low temperatures, similarly to Model 1. However, we note that the yellow curve has two important particularities. First, it nearly superposes to the high density part of the pure Coulomb no-solution curve (green). This trend clearly indicates that both Models coincide in the dense fluid region, where charge order dominates and indifferentiates both models. We will show in the next section that this is equally true for the structural properties as well. The second trend is that the shape of this curve, in particular near the turnover point (square symbol) resembles that of the pure Coulomb curves, particularly visible in the inset through the flattening at very low densities.

It is intriguing that the screened Coulomb interaction of Model 2 should lead to an **nearly** asymptotic temperature limit at the low densities, **quite similar to** the KT transition (red dashed line in the inset of Fig.2). Indeed, since the 2D-Coulomb interaction diverges at large distances, it is understandable that, in the gas limit, all ions become associated into neutral pairs. This flattening effect is not found in the 3D case [36, 37], where it is clearly seen that the temperatures decay with decreasing densities. **However, from theoretical ground, a true KT transition is not expected for Model 2, since free ions will always exist in the limit $\rho \rightarrow 0$ and $T \rightarrow 0$. The nearly flat asymptote indicates that ion pairing in the low density region is different from the 3D case.** The data shown here leads to speculate that charge pairing could be important, even for screened Coulomb interactions, despite the fact that KT transition is not expected to occur for this Model 2.

The second point above lead us to reconsider the low density behaviour of the two models, and in particular that of Model 2. For the 3D case, it has been suggested[33] that the HNC no-solution region is connected to the liquid-gas co-existence, despite the huge difference between the 2 curves, specifically in the low density region. The fact that the screened Coulomb no-solution curve is still considerably above the LG curve suggests that the HNC theory cannot find solutions, not because of the liquid-gas coexistence, but because of clustering connected to charge pairing, which leads to the KT scenario in the case of pure Coulomb interaction. As suggested by the structural properties discussed in sections below, the no-solution curve of HNC corresponds to appearance of correlated dimer clusters, and has nothing to do with the LG binodal. Rather, the no-solution curve of HNC represents a real physical curve, where a particular form of clustering occurs. We conjecture that this state represents a fluid essentially made of polydisperse labile clusters. It represents a fluid different than a liquid of monomers, hence HNC cannot find solutions inside this region. This labile cluster “phase” should contain polydisperse clusters together with free ions exchanging continuously. In this context, HNC would signal a liquid-liquid (or fluid-fluid) transition between two types of disordered liquids/fluids. From this point of view, the turnover point would then be different than a liquid-gas critical point, and would require a new interpretation,

To summarize, it would seem that Model 2 gives a no-solution line which has the same characteristic as Model 1, in particular with a low density turnover point and a tendency to reach an horizontal asymptote for $\rho \rightarrow 0$. This latter point is perhaps the most striking. It shows that charge pairing plays an important role in 2D because of the existence of tightly bound opposite charges, which is a weak remnant of the KT transition which occurs only for Model 1.

3.2 Charge order

Fig.3 shows three snapshots for Model 2, the first two taken above the yellow line of Fig.2, and the last one below, in the no-solution region of HNC. All these snapshots illustrate the charge order, which consists in a local alternation of + and - sites, giving it a **short ranged** “checker-board” aspect. The first shot is taken at high density $\rho = 0.9$ with $\Theta = 0.12$ and the other at low density $\rho = 0.3$ with $\Theta = 0.135$. They both show a rather uniform coverage, despite locally bound + and - pairs. The last one, for $\rho = 0.3$ and $\Theta = 0.09$ shows a less uniform coverage, with apparent large clusters. This looks like a cluster “phase” region, which is inaccessible to HNC. Since computer simulations of Ref.[26] predict equilibrium liquid-gas phase separation well below this parameter region (the black curve in Fig.3 for 2D-RPM), the cluster phase is logically a true thermodynamical phase. The fact that it is inaccessible to HNC, indicates that this integral equation theory

must be adjusted to account for the cluster phase, much the same way it must be adjusted to account for orientationally ordered phases[38, 39]. Since there is no symmetry breaking, we are forced to conclude that HNC points to the existence of a liquid-liquid phase transition, at the blue line in Fig.2 for Model 1, and the yellow line for Model 2.

Fig.4 shows how the various structure functions account for charge order. The pair correlation functions $g_{+-}(r)$ and $g_{++}(r)$ are shown in the 3 main panels, as well as the corresponding structure factors in the insets. The three panels show how these correlations vary as the valence $Z = Z_+ = -Z_-$ is varied from $Z = 0.2$ (leftmost panel), $Z = 0.5$ (central panel) and $Z = 1$ (rightmost panel), this latter valence used in the remainder of the report. Correlations from both models are shown, and are seen to behave very similarly, despite the very different form of the charge-charge interactions. The leftmost panel shows correlations which look very similar to a Lennard-Jones mixture, where all correlations are more or less in phase, while the right most panel shows perfect out-of-phase oscillatory behaviour of the functions $g_{+-}(r)$ and $g_{--}(r)$. This particular behaviour corresponds to an alternate **short ranged** “checker-board” disposition of opposite charged discs. It represents an entire different form of disorder, namely an “ordered form of disorder” which we call charge order. The structure factors reflect this behaviour through the opposite sign peaks at $k\sigma \approx 5$, which corresponds to diagonal distance between 2 discs of same charge in a dense **short ranged** checker-board arrangement of discs. This peak is almost inexistent for $Z = 0.2$ (left panel), where it is the main peak at $k\sigma \approx 2\pi$ which is predominant. The greater amplitude of the first peak of $g_{+-}(r)$ as well as the correspondingly smaller peak for $g_{++}(r)$ in the right panel further illustrate charge order, due to greater contact probability of oppositely charged discs. Another interesting feature is the small k behaviour of $S_{+-}(k)$ and $S_{--}(k)$. The Stillinger-Lovett sum rules, strictly valid only for Model 1, impose $S_{+-}(k=0) = S_{++}(k=0)$. This is verified in all three panels for different values of Z . However, we observe that Model 2 is almost verifying these relations for $Z=1$. This means that configurational charge ordering imposes a near SL sum rule, even though the mathematical form of the structure factors is not strictly obeyed. This is an important information, which will help clarify the low density behaviour in subsequent sections.

3.3 Comparison with computer simulations

Fig.5 shows a comparison between the Monte Carlo simulation and HNC correlation function, for Model 2. It is seen that at low density $\rho = 0.1$, both results are indistinguishable, while marked differences appear at high density of $\rho = 0.9$. These differences are very similar to those found for hard discs, and are likely to represent the approximate diagrammatic nature of HNC -ie- the missing bridge

functions. In view of very good agreement at the low density, it is very likely that HNC reproduces quite accurately the physical behaviour of the model, hence the conjectures made in the previous paragraph are likely to be correct.

3.4 Density dependence

Fig.6 shows how charge ordering changes with density, for both models. Panel (a) represents the charge order shown in Fig.3c, albeit at different state parameters. Panels (b-d) represent how charge order evolves as the density is decreased and the temperature increased. It is seen that the range of charge order correlations decreases with decreasing density, as witnessed by the smaller reach and amplitude of the out-of-phase oscillations. The opposite peaks in the structure factors persist, but with lesser importance, as well a shift to smaller k values. These manifestations are accompanied with a dramatic increase of the first peak of $g_{+-}(r)$ and a nonetheless dramatic flattening of the $g_{++}(r)$ first peak. Fig.(6d) shows that short range charge order has vanished. All these results point to the following configurational behaviour. As the density is decreased, the **short ranged** checker-board order cannot cover the whole configurational space, and because it is restricted to those areas where charges cluster. At very low densities, only dimer clusters exist. The no-solution of HNC marks the limit where the fluid of free particles exist. This is far from a “spinodal” behaviour, which is driven by long range correlations, as in the LG spinodal. It is rather driven by the dramatic increase of the first peak. When rigidly bound pairs form, it is a different physical system, for which the present formulation as free particles is no more valid. So HNC signals a real physical feature, and not a numerical artifact.

3.5 Temperature dependence

Fig.7 for Model 1, and Fig.8 for Model 2, illustrate the temperature dependence of the correlations in (a) the moderately dense fluid at $\rho = 0.5$ and (b) the gas phase region at $\rho = 0.001$. The aim here is to figure out if there is a difference in nature between the high density and low density fluid-fluid transitions, as predicted by the integral equation theory. The main panel of the figures show the running integral $G_{12}(r) = 2\pi \int_0^r s ds [g_{+-}(s) - 1]$ of the cross correlation function $g_{+-}(r)$. It allows to measure how the increase of first peak and short range correlations vary with the increase of the long range tail, as the temperature is decreased towards the no-solution line, at fixed density. Indeed, it is currently admitted that the existence of the no-solution line would correspond to the long range behaviour $g(r) \rightarrow \exp(-r/\xi)/r$, with the correlation length ξ increasing in a peculiar way. For the high density $\rho = 0.5$, the asymptote settles at larger distances as the temperature is decreased. The structure factors in the upper inset are compared at

2 different temperatures, one high $\Theta_1 = 0.18$ and one close to the no-solution boundary $\Theta_1 = 0.07845$. The $k=0$ increase for the latter temperature is clearly seen. The behaviour of $S_{+-}(k=0)$ and the first peak $g_{+-}(\sigma)$ is shown in the lower inset as a function of Θ^{-1} , and confirm that the correlation length increases faster than the first peak. However, Fig.7b shows a different trend at low density $\rho = 0.001$. The main panel shows clearly that the asymptote of $G_{12}(r)$ is reached earlier as the temperature is decreased. The upper inset shows that the structure factors do not show the typical small- k raise. The lower inset shows a marked decrease of both the inverses $1/S_{+-}(k=0)$ and $1/g_{+-}(r_P)$, where r_P is the first peak position, but without the typical turnover that would signal a square-root branching behaviour.

Fig.8 shows the corresponding behaviour for Model 2. While Fig.8a shows that the high density behaviour of Model 2 is similar to Model 1 in Fig.7a, Fig. 8b points to low density differences between the two models. First of all, the asymptote of $G_{12}(r)$ is reached at much smaller distances. This is a direct consequence of the comparison in Fig.6c, where, at $\rho = 0.01$, $g_{+-}(r)$ for Model 1 is seen to have a wider decay than for Model 2. However, the temperature dependence of the reach of the asymptote is similar to Model 1. The top inset shows that there is no $k=0$ raise anomaly, again similarly to Model 1. The Stillinger-Lovett laws are not obeyed, as expected. The lower inset shows a sharper drop of the inverses $1/S_{+-}(k=0)$ and $1/g_{+-}(r_P)$ than for Model 1 in Fig.7b. Our interpretation of these low density differences between the two models is that the Stillinger-Lovett conditions, constrain enormously the behaviour of the long range shape of $g_{+-}(r)$, as well that of small k behaviour of $S_{+-}(k)$. This is due to the long range nature of the Coulomb interaction in Model 1, which is missing in Model 2. However, the charge pairing, which is dictated solely by the short range part of the interaction, exist in both models, and conditions the same way the formation of neutral dimers. It is the formation of higher clusters which may be different in both models, necessitating lower temperatures for Model 2 in order to compare with Model 1. This may explain that the KT-like shape of the no-solution curve (yellow) appears shifted to the lower part of the phase diagram of Fig.2, as compared to Model 1 (blue).

4 Discussion

Aside the [short ranged](#) checker board type charge ordering, which seems to dominate in both models studied here, perhaps the most interesting part is the fate of these systems in the very low density region, where they all seem to indicate the existence of a lower cluster phase, dielectric for Model 1, but with high density of dipoles for Model 2. The mechanism for loss of solution of the HNC theory

is the same for both models: it is the dramatic raise of the first peak of $g_{+-}(r)$ which is due to charge pairing. Interestingly, there is no marked signature of the small- k increase of the structure factors, typical of the LG spinodal. In any case, it is certain that it is charge pairing which destabilises the free charge phase into a dielectric phase. Therefore, it is not a surprise that both models, which predict charge pairing at high densities, equally predict this pairing at lower densities. The universality of the KT transition is solely due to the Coulomb form and is related to the appearance of a dielectric phase. The screened Coulomb form interaction, because of the lack of long range, does not allow a full dielectric phase, since many free charges might exist even at low temperature. So the KT transition for such interactions is out-ruled. However, the similarity of the no-solution lines for HNC suggest that strong clustering cannot be described by this theory. Hence it may represent a new phase, such as a labile cluster phase. The snapshot in Fig.3 suggest this difference.

The second interesting point suggested by the present study, is the possibility of a fluid-fluid transition below the no-solution region of HNC. While this transition is acceptable in the low density region, because of the formation of the dielectric phase, it is less obvious in the high density region, where it could be possible that the no-solution curve would be only the premise of the LG coexistence predicted by simulations[26]. Both Fig.7a and Fig.8a point to such scenario. However, the no-solution curve for HNC is quite above the LG coexistence curve of the simulations. This is also the case for the 3D RPM. Moreover, in 3D, very close to the no-solution line, the results of HNC are remarkably in agreement with those of the simulations, at least for the soft-core RPM[7]. This agreement is deteriorated in the present 2D results, principally because of the increased fluctuations due to the reduced dimensionality. Nevertheless, these results point to the possible existence of a cluster phase below the no-solution line, as shown in Fig.3c. This phase could be made mostly of dimers in the very low density region, leading to the KT pairing scenario, while leading to higher clusters in the high density region. Then, the liquid part of LG coexistence curve would be the result of a collapse of a fluid of aggregates into a denser liquid. One additional evidence for an intermediate cluster phase is indirectly provided by studied of the ultra-soft RPM in the 3D case[40], studied both from computer simulations and approximate mean field theories taking into account various levels of ionic association. The results of Ref.[40] seems to indicate that all the theoretical (ρ, Θ) curves lie above that phase diagram determined by computer simulations, just like in the present case. The impossibility of reaching the true binodal could be an indirect evidence that the cluster phase needs to be explicitly taken into account.

If we admit the existence of a fluid-fluid transition, one question would be how to detect it through thermodynamic considerations. The wide literature in the low density region of the KT transition, indicate that this would be a transition of

infinite order, with no usual thermodynamic signature. Studies of heat capacity in the 3D case indicate the existence of a weak bump anomaly above the LG transition[41]. It is obvious that more investigations are required, and we hope that the present work would stimulate them.

5 Conclusion

The present works indicates that charge ordering holds both for pure 2D-Coulomb and screened 3D-Coulomb forms of the interaction. It is enough that large amplitude short range interactions exist. This is analogous to the screened Coulomb interaction, in other words massive interactions versus massless interactions, to borrow a Condensed Matter Physics modern language, where the parameter $1/\lambda$ in Eq.(4) plays the role of a “mass”[1]. In this context, it was interesting to address the problem of charge ordering in two-dimensions, where peculiarities such as the KT transitions are known to exist. We report evidence for a transition for massive interactions, as separating differently clustered free charge region of the phase diagram. The strict dimer dielectric phase would then be a particular case, when all charges in the lower phase are bound in pairs. Furthermore, it would seem that an approximate theory such as the HNC closure, is be able to predict the solution boundary of this phase separation. Most of the interesting physics, as discovered by other authors, such as LG binodal or conducting-dielectric transition, lies below the region accessible to the HNC theory. This observation opens the grounds to extend this approximation to this region, by considering explicitly bound charge pairs, for example. The concept of charge order can equally extended to more complex molecular models, following insights gained in the three-dimensional case. Finally, the confirmation through other methods of the existence of a fluid-fluid transition requires further investigations of simple two-dimensional ionic liquids.

Acknowledgements

This work was funded in parts by the French-Slovenian PROTEUS project N° 35120VG. TU acknowledges the support by the NIH (GM063592) and Slovenian Research Agency (P1 0103-0201, N1-0042).

References

- [1] P.M. Chaikin and T.C. Lubensky, Principles of condensed matter physics, Cambridge University Press, 1995.
- [2] N. D. Mermin and H. Wagner, Phys. Rev. Lett. **17**, 1133 (1966)
- [3] J. M. Caillol, D. Levesque, J. J. Weis, and J. P. Hansen , J. Stat. Phys. **28**, 325 (1982)
- [4] J. P. Hansen, Phys. A **140**, 150 (1986)
- [5] J. E. Enderby and G. W. Neilson, Rep. Prog. Phys., **44**, 38 (1981)
- [6] J. M. Kosterlitz and D. J. Thouless, J. Phys. C : Solid State Phys. **6** , 1181 (1973)
- [7] A. Perera and R. Mazighi. J. Mol. Liq. 210, 243 (2015)
- [8] A. Perera. Phys. Chem. Chem. Phys., **19**, 1062, (2017).
- [9] C.A. Angell, Y. Asnsari, Z. Zhao, Faraday Discuss. **154** (2012) 9.
- [10] F. Lado, J. Chem. Phys. 49,3092 (1988).
- [11] P.G. Ferreira, A. Perera, M. Moreau and M. M. Telo da Gama, J. Chem. Phys. **95**, 7591 (1991)
- [12] A. Perera, Mol. Phys. **107**, 487 (2009)
- [13] J.K. Percus, J. Stat. Phys. **15**, 505 (1976).
- [14] J. S. Høye and K. Olaussen, Physica A **104**, 447 (1980)
- [15] Y. Levin, X.-J. Li, and M. E. Fisher, Phys. Rev. Lett. **73**, 2716 (1994)
- [16] A. Fortini, A.-P. Hynninen, and M. Dijkstra , J. Chem. Phys. **125**, 094502 (2006)
- [17] J.-M. Caillol, F. Lo Verso, E. Schöll-Pashinger and J. J. Weis, Mol. Phys. **105**, 1813 (2008)
- [18] L. Samaj and I. Travenec, J. Stat. Phys. **101**, 713 (2000)
- [19] J. P. Hansen and P. Viot, J. Stat. Phys. **38**, 823 (1985)
- [20] W.-K. Chung and S. S. Mak, Chem. Phys. 155, 19 (1991)

- [21] E. Lomba, J. J. Weis, and F. Lado, *J. Chem. Phys.* **127**, 074501 (2007).
- [22] P. Pršlja, J. Aupič, Jana, T. Urbic, *Mol. Phys.*, **115**, 1572 (2017)
- [23] J. Aupič, Jana, T. Urbic, *J. Chem. Phys.* **140**, 184509 (2014)
- [24] T. Urbic and V. Vlachy, *Acta Chim. Slov.* **46**, 531 (1999)
- [25] J. Aupic and T. Urbic, *J. Chem. Phys.* **142**, 014506 (2015)
- [26] G. Orkoulas and A. Z. Panagiotopoulos, *J. Chem. Phys.* **104**, 7205 (1996).
- [27] P. Minnhagen, *Rev. Mod. Phys.* **59**, 1001 (1987).
- [28] Z. Gulàcsi and M. Gulàcsi, *Adv. Phys.* **47**, 1 (1998)
- [29] J. D. Talman, *J. Comput. Phys.* **29**, 35 (1978)
- [30] P. G. Ferreira, A. Perera, M. Moreau, M. M. Telo da Gama. *J. Chem. Phys.* **95**, 7591 (1991).
- [31] J. P. Hansen, I. R. McDonald. *Theory of Simple Liquids*, Academic, London (1986).
- [32] F. H. Stillinger and R. Lovett, *J. Chem. Phys.* **48**, 3858 (1968)
- [33] L. Belloni, *J. Chem. Phys.* **98**, 8080 (1993)
- [34] D. Frenkel and B. Smit, *Molecular simulation: From Algorithms to Applications*, (Academic Press, New York, 2000).
- [35] C. Valeriani, P. J. Camp, J. W. Zwanikken, R. van Rij and M. Dijkstra, *Soft Matter* **6**, 2793 (2010)
- [36] P. J. Camp and G. N. Patey, *Phys. Rev. E* **60**, 1063 (1999)
- [37] C. Valeriani, P. J. Camp, J. W. Zwanikken, R. van Roij and M. Dijkstra, *Soft Matter* **6**, 2793 (2010)
- [38] F. Lado and E. Lomba, *Phys. Rev. Lett.* **80**, 3535 (1998).
- [39] A. Perera. *Phys. Rev.* **E60**, 2912 (1999).
- [40] A. Nikoubashman, J.-P. Hansen, and G. Kahl, *J. Chem. Phys.* **137**, 094905 (2012)
- [41] P. J. Camp and G. N. Patey, *J. Chem. Phys.* **111**, 9000 (1999)

Figure Captions

- Fig.1 Terms of the interactions in Model 1 and 2 in Eqs.(3,4). The blue curve represents the $1/r$ interaction, the magenta curve the 2D Coulomb interaction between charges of opposite signs, and the green curves represent the Yukawa term, green for $\lambda = 2$ and dark green for $\lambda = 1$.
- Fig.2 Phase diagram (ρ, θ) . The black and red curves are, respectively, the liquid-gas binodal and the conductor-dielectric boundary, as determined from computer simulations[26] for the 2D-RPM. The blue curve is the HNC no-solution line for the 2D-RPM[21]. The green and yellow curves are the HNC no-solution lines from this work, for Model 1 and Model 2, respectively. The inset is a zoom on the low density behaviour, with logarithmic scale for the density. The red dashed line shows the KT asymptote.
- Fig.3 Snapshots of Model 2 for 3 different conditions. (a) Dense fluid $\rho = 0.9$ and $\Theta = 0.12$; (b) low density hot fluid $\rho = 0.1$ and $\Theta = 0.135$; (c) Cluster phase below the non-solution region $\rho = 0.3$ and $\Theta = 0.09$.
- Fig.4 Valence dependence of charge ordering at density $\rho = 0.9$ for Model 1 ($\Theta_1 = 0.045$) and Model 2 ($\Theta_2 = 0.1$), as determined by the HNC approximation. (a) $Z=0.2$, (b) $Z=0.5$ and (c) $Z=1$. Model 1: blue curve for $g_{++}(r)$ and magenta for $g_{+-}(r)$. Model 2: green curve for $g_{++}(r)$ and gold for $g_{+-}(r)$. The insets represent the corresponding structure factors $S_{ij}(k)$ with same color conventions.
- Fig.5 Comparison with simulations for Model 2 for $\Theta_2 = 0.16$, $\rho = 0.9$ (main panel) and $\rho = 0.1$ (inset). HNC: blue curve for $g_{++}(r)$ and magenta for $g_{+-}(r)$. Simulations: green curve for $g_{++}(r)$ and gold for $g_{+-}(r)$.
- Fig.6 Density dependence of charge order for Model 1 and Model 2, close to their respective no-solution curve for HNC. Line conventions: Model 1: ++ in blue and +- in magenta; Model 2: ++ in green and +- in gold. (a) $\rho = 0.8$, $\Theta_1 = \Theta_2 = 0.054$; (b) $\rho = 0.3$, $\Theta_1 = 0.1436$ and $\Theta_2 = 0.108$; (c) $\rho = 0.1$, $\Theta_1 = 0.2$ and $\Theta_2 = 0.135$; (d) $\rho = 0.01$, $\Theta_1 = 0.36$ and $\Theta_2 = 0.135$.
- Fig.7 Temperature dependence of structure parameters for Model 1. (a) Main panel: running KBI $G_{+-}(r)$ for $\rho = 0.5$ and for different tem-

peratures; from bottom to top $\Theta_1 = 0.18, 0.09, 0.08, 0.079$ and 0.07845 . Top inset shows $S_{++}(k)$ (upper set of curves) and $S_{+-}(k)$ (lower set of curves) for $\Theta_1 = 0.18$ (blue) and $\Theta_1 = 0.07845$ (magenta). Lower inset shows Θ -dependence of $1/S_{+-}(0)$ (blue) and inverse of first peak of g_{+-} (magenta). (b) Similar data as (a), but for very low density $\rho = 0.001$. Temperatures in the main panel are $\Theta_1 = 0.9, 0.72, 0.54$ and 0.53 . Upper inset $S_{++}(k)$ (upper set) and $S_{+-}(k)$ (lower set) for $\Theta_1 = 0.9$ (blue) and $\Theta_1 = 0.53$ (magenta). Lower inset, same as in (a).

Fig.8 Temperature dependence of structure parameters for Model 2. (a) Main panel: running KBI $G_{+-}(r)$ for $\rho = 0.5$ and for different temperatures; from bottom to top $\Theta_2 = 0.8, 0.27, 0.16, 0.10, 0.096, 0.086$ and 0.082 . Top inset shows $S_{++}(k)$ (blue) and $S_{+-}(k)$ (magenta) for $\Theta_1 = 0.18$ (blue) and $\Theta_1 = 0.085$ (magenta). Lower inset shows Θ -dependence of $1/S_{+-}(0)$ (blue) and inverse of first peak of g_{+-} (magenta). (b) Similar data as (a), but for very low density $\rho = 0.001$. Temperatures in the main panel are $\Theta_1 = 0.8, 0.27, 0.16$ and 0.10 . Upper inset $S_{++}(k)$ (blue) and $S_{+-}(k)$ (magenta) for $\Theta_1 = 0.8$ (blue) and $\Theta_1 = 0.10$ (magenta). Lower inset, same as in (a).

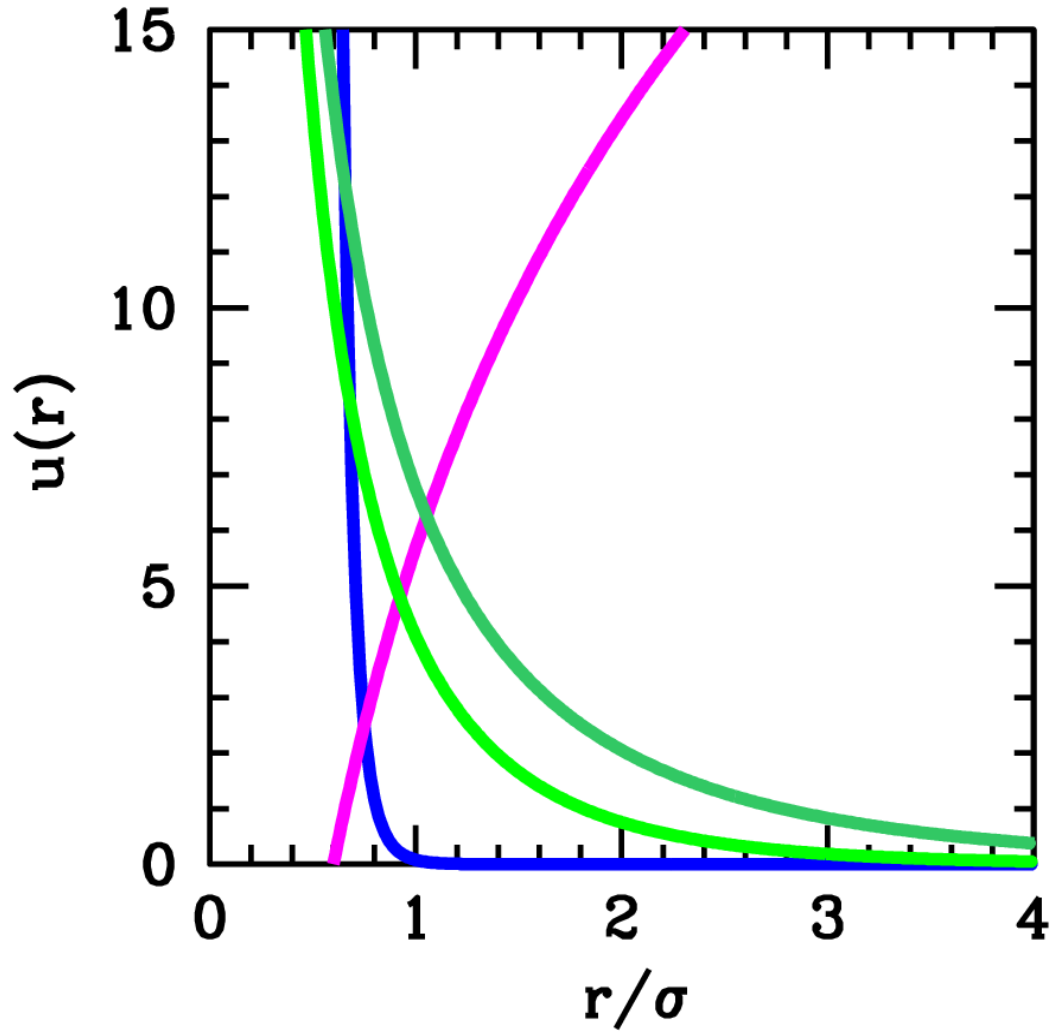


Fig.1- Terms of the interactions in Model 1 and 2 in Eqs.(3,4). The blue curve represents the $1/r^{12}$ interaction, the magenta curve the 2D Coulomb interaction between charges of opposite signs, and the green curves represent the Yukawa term, green for $\lambda = 2$ and dark green for $\lambda = 1$.

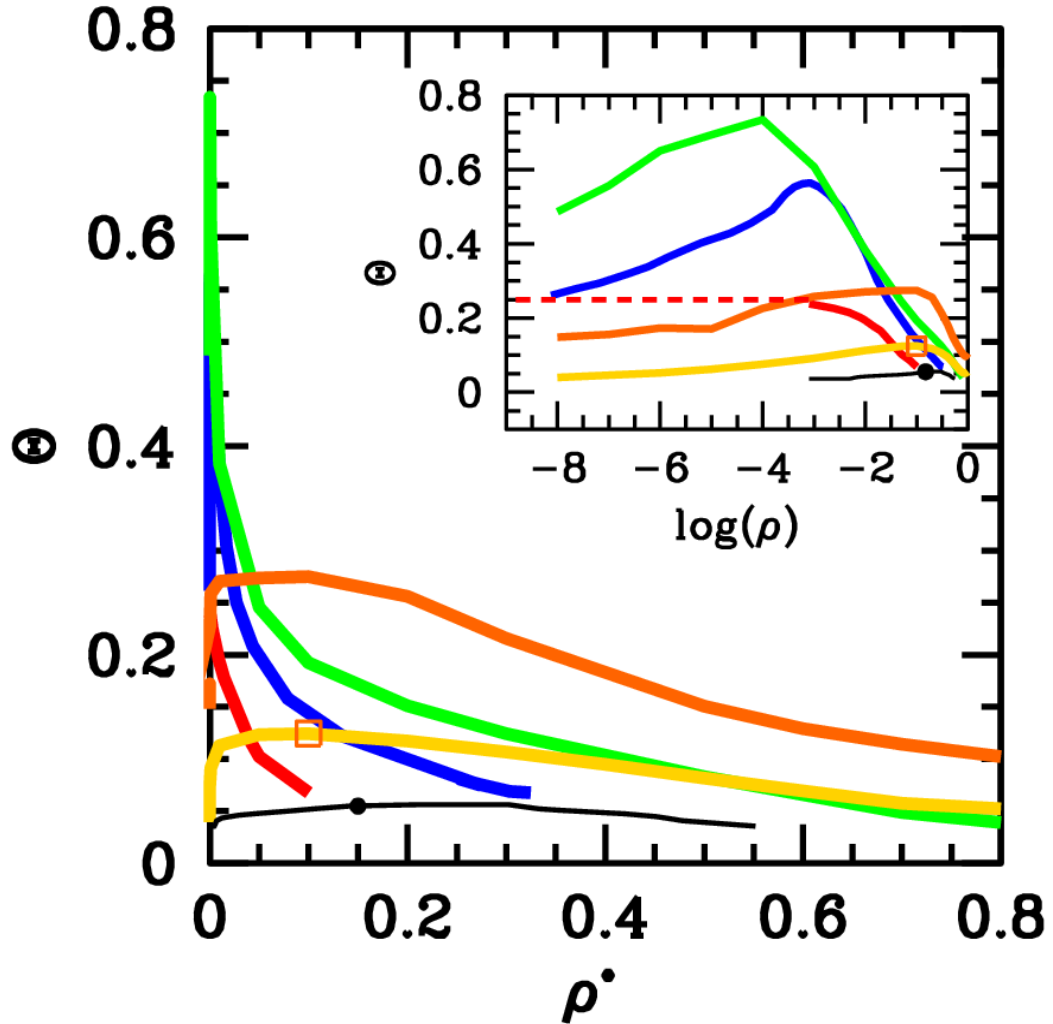


Fig.2 Phase diagram (ρ, θ) . The black and red curves are, respectively, the liquid-gas binodal and the conductor-dielectric boundary, as determined from computer simulations[26] for the 2D-RPM. The blue curve is the HNC no-solution line for the 2D-RPM[21]. The green and yellow curves are the HNC no-solution lines from this work, for Model 1 and Model 2, respectively. The inset is a zoom on the low density behaviour, with logarithmic scale for the density. The red dashed line shows the KT asymptote.

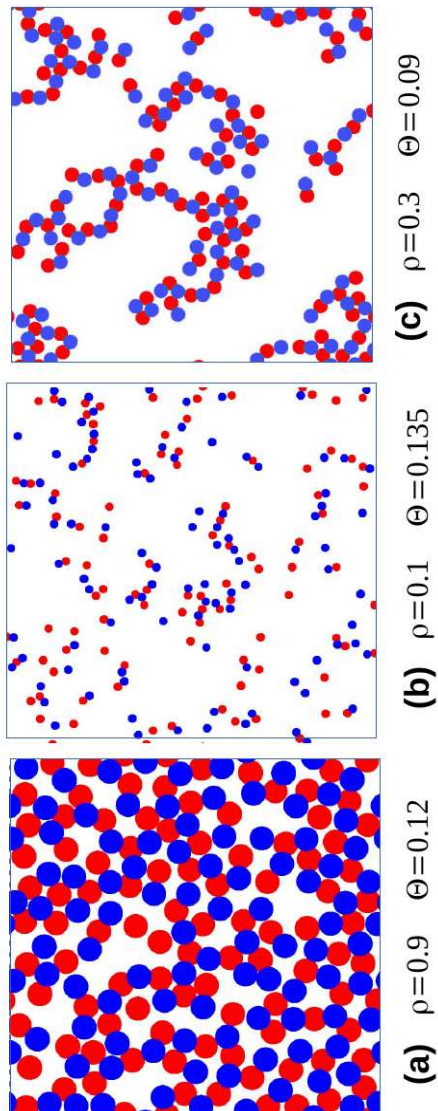


Fig.3 - Snapshots of Model 2 for 3 different conditions. (a) Dense fluid $\rho = 0.9$ and $\Theta = 0.12$; (b) low density hot fluid $\rho = 0.1$ and $\Theta = 0.135$; (c) Cluster phase below the non-solution region $\rho = 0.3$ and $\Theta = 0.09$.

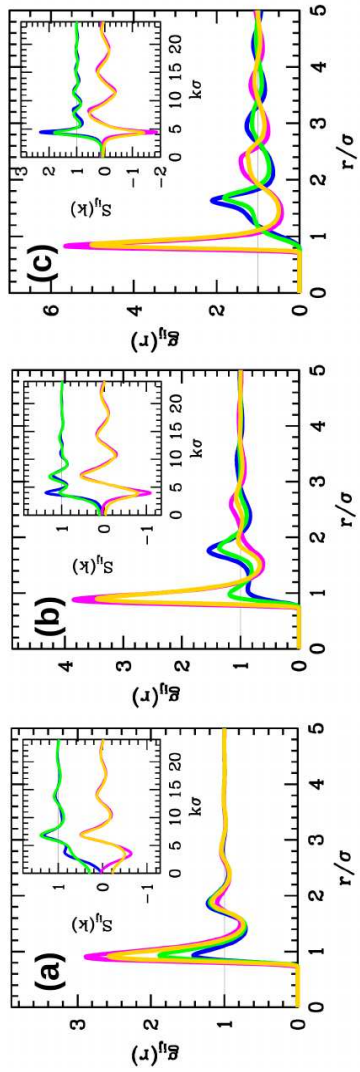


Fig.4 - Valence dependence of charge ordering at density $\rho = 0.9$ for Model 1 ($\Theta_1 = 0.045$) and Model 2 ($\Theta_2 = 0.1$), as determined by the HNC approximation. (a) $Z=0.2$, (b) $Z=0.5$ and (c) $Z=1$. Model 1: blue curve for $g_{++}(r)$ and magenta for $g_{+-}(r)$. Model 2: green curve for $g_{++}(r)$ and gold for $g_{+-}(r)$. The insets represent the corresponding structure factors $S_{ij}(k)$ with same color conventions.

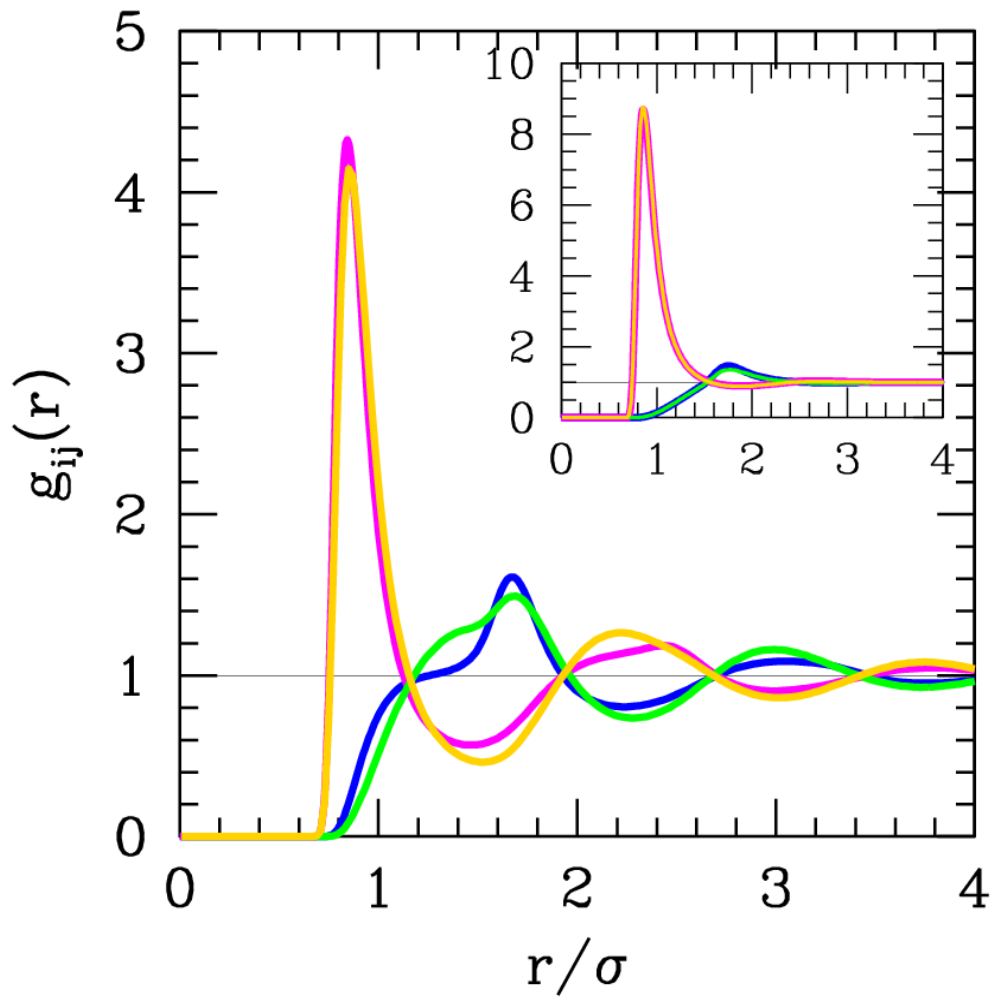


Fig.5 Comparison with simulations for Model 2 for $\Theta_2 = 0.16$, $\rho = 0.9$ (main panel) and $\rho = 0.1$ (inset). HNC: blue curve for $g_{++}(r)$ and magenta for $g_{+-}(r)$. Simulations: green curve for $g_{++}(r)$ and gold for $g_{+-}(r)$..

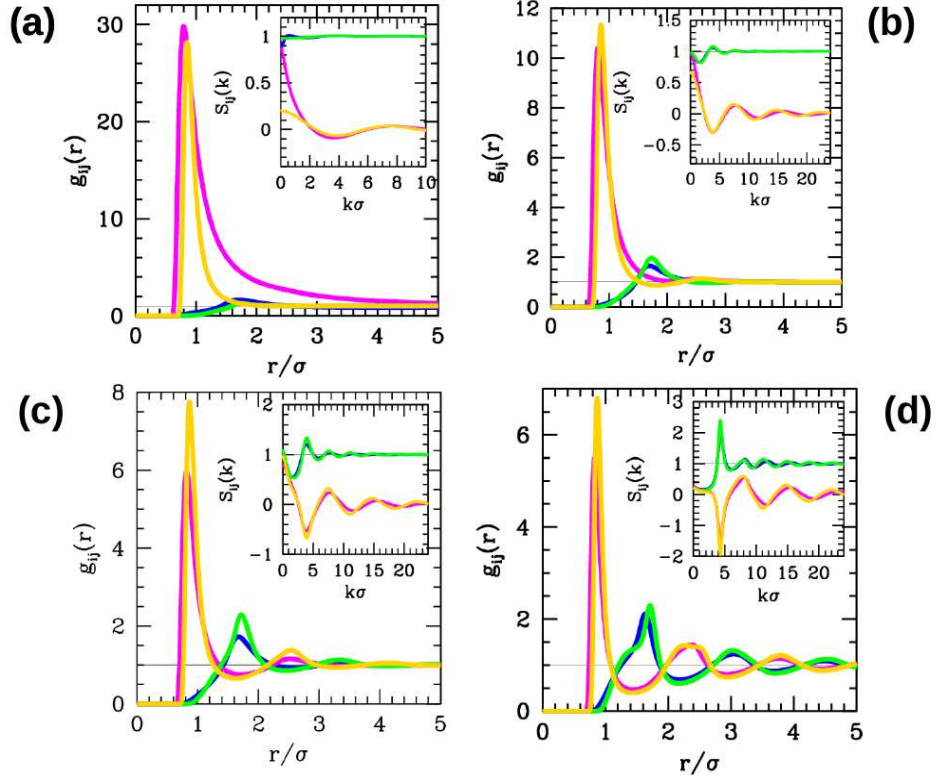


Fig.6 - Density dependence of charge order for Model 1 and Model 2, close to their respective no-solution curve for HNC. Line conventions: Model 1: ++ in blue and +- in magenta; Model 2: ++ in green and +- in gold. (a) $\rho = 0.8$, $\Theta_1 = \Theta_2 = 0.054$; (b) $\rho = 0.3$, $\Theta_1 = 0.1436$ and $\Theta_2 = 0.108$; (c) $\rho = 0.1$, $\Theta_1 = 0.2$ and $\Theta_2 = 0.135$; (d) $\rho = 0.01$, $\Theta_1 = 0.36$ and $\Theta_2 = 0.135$.

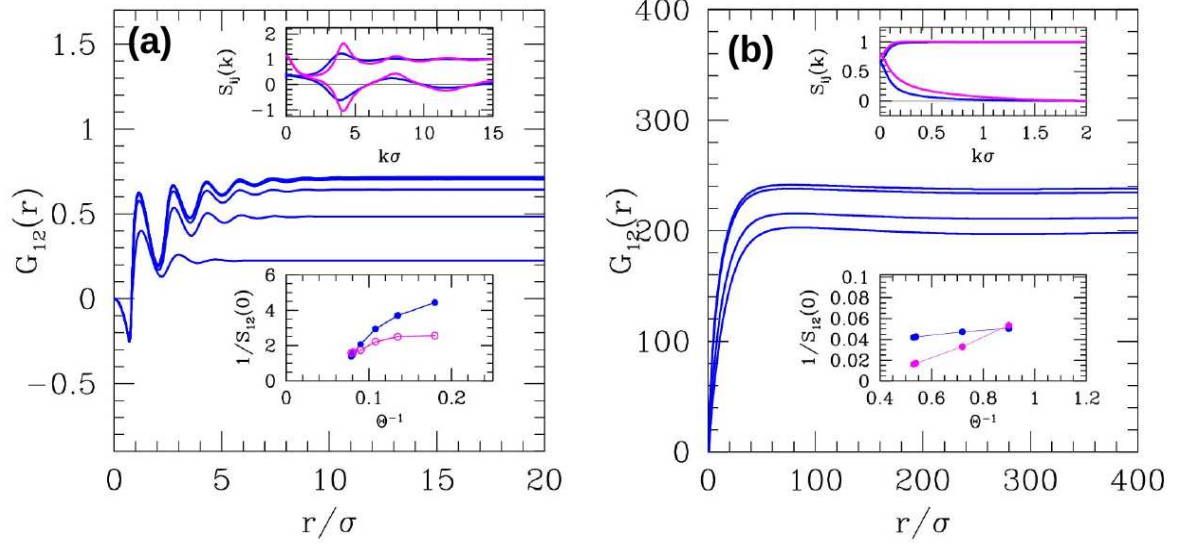


Fig.7 - Temperature dependence for Model 1. (a) Main panel: running KBI $G_{+-}(r)$ for $\rho = 0.5$ and for different temperatures; from bottom to top $\Theta_1 = 0.18, 0.09, 0.08, 0.079$ and 0.07845 . Top inset shows $S_{++}(k)$ (blue) and $S_{+-}(k)$ (magenta) for $\Theta_1 = 0.18$ (blue) and $\Theta_1 = 0.07845$ (magenta). Lower inset shows Θ -dependence of $1/S_{+-}(0)$ (blue) and inverse of first peak of g_{+-} (magenta). (b) Similar data as (a), but for very low density $\rho = 0.001$. Temperatures in the main panel $\Theta_1 = 0.9, 0.72, 0.54$ and 0.53 . Upper inset $S_{ij}(k)$ (blue) and $S_{+-}(k)$ (magenta) for $\Theta_1 = 0.9$ (blue) and $\Theta_1 = 0.53$ (magenta). Lower inset :same as in (a).

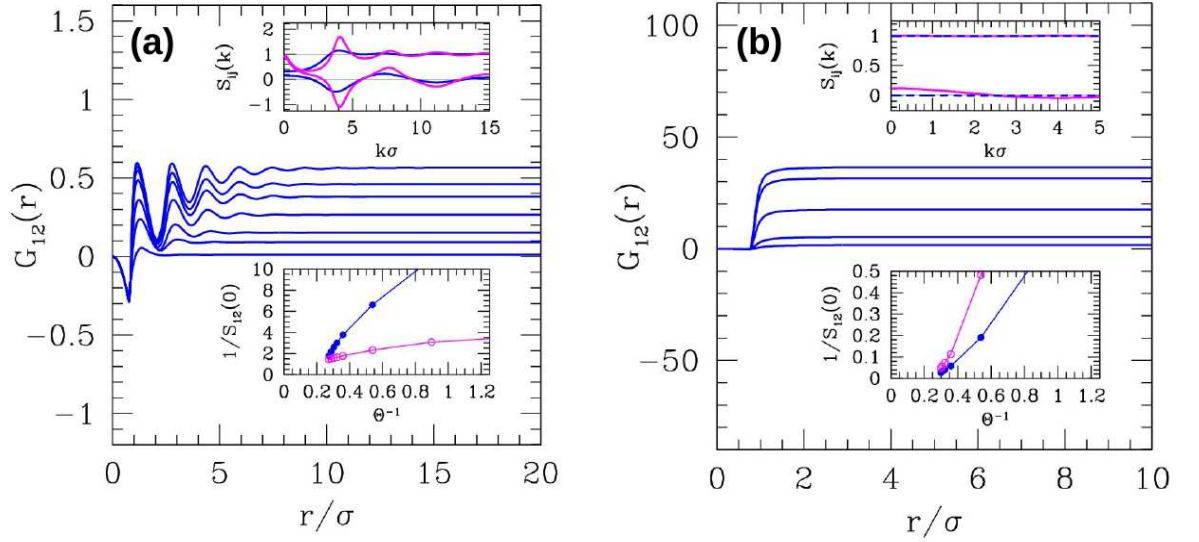


Fig.8 - Temperature dependence for Model 2. (a) Main panel: running KBI $G_{+-}(r)$ for $\rho = 0.5$ and for different temperatures; from bottom to top $\Theta_2 = 0.8, 0.27, 0.16, 0.10, 0.096, 0.086$ and 0.082 . Top inset shows $S_{++}(k)$ (blue) and $S_{+-}(k)$ (magenta) for $\Theta_1 = 0.18$ (blue) and $\Theta_1 = 0.085$ (magenta). Lower inset shows Θ -dependence of $1/S_{+-}(0)$ (blue) and inverse of first peak of g_{+-} (magenta). (b) Similar data as (a), but for very low density $\rho = 0.001$. Temperatures in the main panel $\Theta_1 = 0.8, 0.27, 0.16$ and 0.10 . Upper inset $S_{ij}(k)$ (blue) and $S_{+-}(k)$ (magenta) for $\Theta_1 = 0.8$ (blue) and $\Theta_1 = 0.10$ (magenta). Lower inset :same as in (a).